doi.org/10.26434/chemrxiv.7127066.v1

Inkjet-Printed Mesoporous TiO2 and Perovskite Layers for High Efficiency Perovskite Solar Cells

Aron Huckaba, Yonghui Lee, Rui Xia, Sanghyun Paek, Victor Costa Bassetto, Emad Oveisi, Andreas Lesch, Sachin Kinge, Paul Dyson, Hubert Girault, Mohammad Khaja Nazeeruddin

Submitted date: 25/09/2018 • Posted date: 25/09/2018

Citation information: Huckaba, Aron; Lee, Yonghui; Xia, Rui; Paek, Sanghyun; Costa Bassetto, Victor; Oveisi, Emad; et al. (2018): Inkjet-Printed Mesoporous TiO2 and Perovskite Layers for High Efficiency Perovskite Solar Cells. ChemRxiv. Preprint.

Inks for the inkjet-deposition of Titanium dioxide and hybrid organic inorganic perovskites were synthesized and then used to deposit films for high efficiency perovskite solar cell devices. The inkjet-printed titanium dioxide electron transport layer was optimized in reference to state-of-the-art spin-coated tio2 films. After observing that the printed TiO2 films perform at least as well as the spin-coated version, this charge transport layer was used as the anode for inkjet-printed perovskite absorber layers. Using printed TiO2 and perovskite, 14.1% power conversion efficiency was achieved.

File list (2)

Inkjet-Printed Mesoporous TiO_2 and Perovskite Layers for High Efficiency Perovskite Solar Cells

Aron J. Huckaba,[a,*] Yonghui Lee,[a] Rui Xia,[a,b] Sanghyun Paek,[a] Victor Costa Bassetto,[c] Emad Oveisi,[d] Andreas Lesch,[c] Sachin Kinge,[e] Paul J. Dyson,[b] Hubert Girault,[c] Mohammad Khaja Nazeeruddin[a],*

a: GMF, Institute of Chemical Sciences and Engineering, EPFL Valais-Wallis, Rue de l'industrie 17, 1951 Sion, Switzerland.

b: Institute of Chemical Sciences and Engineering, Ecole Polytechnique Fédérale de Lausanne (EPFL), CH-1015 Lausanne, Switzerland.

c: LEPA, Institute of Chemical Sciences and Engineering, EPFL Valais-Wallis, Rue de l'industrie 17, 1951 Sion, Switzerland.

d: Interdisciplinary Centre for Electron Microscopy, EPFL, 1015 Lausanne, Switzerland

e: Toyota Motor Corporation, Toyota Motor Technical Centre, Advanced Technology Div., Hoge Wei 33, B-1930 Zaventum, Belgium.

Abstract

Perovskite solar cells with mesoporous TiO_2 electron transport layers have previously reached >22% efficiency at the laboratory scale (<1 cm^2), however, these layers are fabricated using spin-coating, which is not conducive to large-scale or high throughput fabrication. This report describes the inkjet printing of open-pore mesoporous TiO_2 thin films, perovskite thin films, and the fabrication of highly efficient perovskite solar cells using these films. Ink formulation and characterization studies, inkjet deposition optimization trials, film characterization, and comparison to spin-coated layers are described. The printed TiO_2 films exhibited an open-pore morphology and homogeneous surface coverage in films ranging from 1 mm^2 to >10 cm^2. Perovskite solar cells with printed and pristine (undoped) inkjet-printed TiO_2 layers yielded efficiencies of 18.29%, which were found to outperform cells made with spin-coated and

pristine TiO_2 layers (16.91%). When a quadruple-cation perovskite absorber containing Cs, formamidinium, methylammonium, and guanidinium was deposited by inkjet-printing onto the inkjet-printed TiO_2 layer, nearly 12% average efficiency was reached, with the champion cell reaching 14.11%. This absorber exhibited higher efficiency and stability than did inkjet-printed $MAPbI_3$ films deposited on the inkjet-printed TiO_2 film.

Introduction

Since the seminal report in 2009, the highest efficiency perovskite solar cells have risen from 3.8% to greater than 23%.[1] The highest performing devices typically have small areas (<1 cm^2) and are fabricated by spin-coating deposition of most of the active layers.[2] While spin-coating works well for small area substrates, it is not industrially applicable due to the high percentage of material loss and substrate size limitation .[3] Reports of perovskite absorber layer deposition by industrially relevant techniques such as slot-die coating,[4] evaporation,[5] and inkjet printing[6] are becoming more frequent. Of these methods, printed mesoscopic perovskite solar cells have been reported to last >10,000 h without notable performance losses.[7]

Inkjet printing is a digital, mask-less and contact-less fabrication technique that allows the direct deposition of miniscule ink volumes onto substrates with full pattern control, where the pattern resolution is limited by the droplet volume (generally below 100 pL) and the spreading diameter of the droplet on the substrate.[8] Complete Organic Light Emitting Diodes (OLEDs),[9] Field Effect Transistors (FETs),[10] and Organic Phtovoltaic (OPV)[11] devices have been fabricated using inkjet printing, but this has not yet been achieved with perovskite solar cells.[12] Inkjet-printed perovskite absorber layers have been reported,[13–15] as have slot die printed perovskite and electron transport layers.[4] Other active layers relevant to perovskite

solar cells, such as various electron transport materials (ETM, such as ZnO,[16] SnO_2,[17] TiO_2)[18,19] and hole transport materials (HTM, such as poly(3,4-ethylenedioxythiophene) polystyrene sulfonate (PEDOT:PSS)[16] have also been inkjet-printed and applied in various devices. In piezoelectric drop on-demand (DOD) inkjet printing, droplets are ejected by a pressure pulse generated in a fluid filled cavity by a piezoelectric actuator (Figure 1a). The implementation of several hundred individually addressable nozzles, jetting frequencies in the kHz range and the possibility of multiple printing passes allows for fast thin film production and integration of inkjet printheads into roll-to-roll devices. The precise control of the number of printed layers and the lateral droplet density allows the construction of nanometer to micrometer thick films.

The precursor to perovskite solar cells, dye-sensitized solar cells, relies on several micrometer (~10 μm) thick layers of TiO_2.[20] Similarly, mesoscopic perovskite cells also utilize many hundreds of nanometers thick metal oxide layers.[2,7] High efficiency perovskite solar cells with a mesoscopic architecture are reported to have a ~150 nm thick layer of TiO_2, which is normally deposited by spin-coating deposition.[21] While there are many papers describing spin-coating deposition of mesoporous TiO_2, reports describing deposition by inkjet printing are sparse.[18,19,22–24] Because we believe the development of an industrially relevant and scalable deposition method for mesoporous TiO_2 films will be useful for the commercialization of perovskite solar cells, we sought to develop an inkjet printing method of deposition for mesoporous TiO_2 and apply them in perovskite solar cells. We report, herein, high efficiency perovskite solar cells with DOD inkjet-printed mesoporous TiO_2 layer exhibiting power conversion efficiencies >18%. The devices utilized compact TiO_2 and inkjet-printed TiO_2 as ETL and Spiro-MeOTAD as HTL (Figure 1b). The ink could be printed over large areas and the obtained TiO_2 films did not require doping to achieve high efficiency devices (Figure 1c).

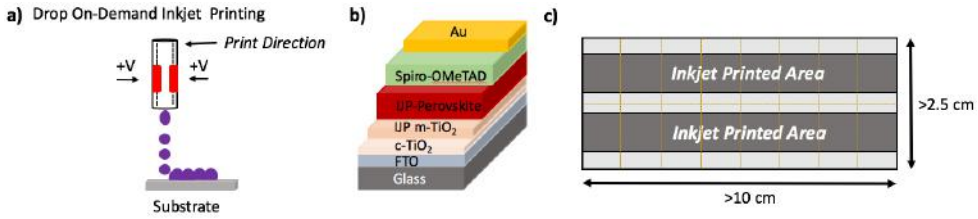

Figure 1. *a)* Principle of operation of a piezoelectric DOD inkjet printer. *b*)Cross sectional device schematic of solar cell devices fabricated in this study, with the inkjet printed (IJP) m-TiO_2 and perovskite absorber layer indicated. *c)* Top view illustration of the printed m-TiO_2 substrate area, with individual devices marked in dashed lines.

Results and Discussion

Ink Formulation

Experimentally, the optimized ink composition was found to consist of three important parts: high viscosity solvent, low viscosity solvent, and humectant (Table 1). For inkjet printing, viscosity, surface tension and density of the ink are important, while the vapor pressure influences the drying time and final quality of the film. The humectant is important to minimize ink evaporation and clogging at the nozzle opening. To circumvent the coffee-ring effect,[8] we chose solvents with a low vapor pressure and high polarity to obtain stable droplet edge pinning to the substrate edge with controlled evaporation to yield a uniform layer of nanoparticles with minimal particle migration.[23] N,N-dimethylformamide (DMF) was chosen to increase the rate of drying over water,[23] and cyclohexanol was chosen for its high viscosity and moderately polar nature.

While some reports of inkjet-printed TiO_2 layers have utilized P25 TiO_2,[18,23] we found that while inks prepared with Degussa powder led to reasonably stable ink suspensions (>6 h stable), solar cell performance could not be optimized to greater than ~13% power conversion efficiency (PCE). Another report utilized an aqueous dispersion of a commercial TiO_2 paste,[19]

but in our hands these suspensions were not stable enough to print effectively. We chose to utilize a non-aqueous ink with GreatCell Solar Italia (formerly DyeSol) 30NRT dye paste as our TiO_2 source. No surfactants or pH modifying additives were required in this ink formulation.

The formulated ink exhibited a dynamic viscosity value (14.1 mPa·s, 25ºC, Table S1) within the acceptable range of viscosity for DOD inkjet printing (2-20 mPa·s), even up to 70ºC (Figure S1).[25] Increasing the ink temperature led to a decrease in dynamic viscosity from 14.1 mPa·s at 25ºC to 4.17 mPa·s at 68ºC. The surface tension (32.7 dynes·cm^{-1}) was measured by the pendant drop method and was observed to be acceptable for DOD inkjet printing.

Measuring the contact angle of a deposited sessile drop on a compact TiO_2 surface indicated a contact angle of 20.3º, which indicated good wettability and spreading, which is advantageous for uniformly covering the surface (Figure S2a). During printing, stable and spherical droplets without satellites and without tail formed within 45 μs after ~100 μm of flight (Figure S2b). The droplet volume was observed to be 7.91 ± 1.36 pL with a diameter of 24.6 ± 1.40 μm. When printing the ink on a cleaned compact TiO_2 surface, good surface coverage was observed with no pinholes (Figure S2c).

TiO_2 Film Morphology

In DOD inkjet printing, two factors affect film thickness when the concentration of solid material is kept constant, especially as it pertains to nanoparticles: drop spacing and numbers of layers deposited (Figure 2).

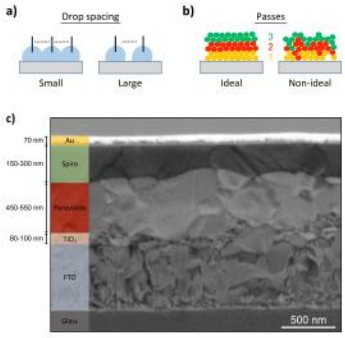

Figure 2. Conceptual depiction of *a)* drop spacing of ink droplets as it pertains to surface coverage. Dashed line is the same length for both examples. *b)* Multi-pass inkjet printing and ideal/non-ideal surface coverage of printed nanoparticles after ink carrier evaporation and indicating in different color codes subsequently printed each layer. *c*) Scanning electron microscope image of device cross section (drop spacing = 30 μm, passes = two).

Drop spacing is defined as the distance between the center of two adjacent droplets on the substrate and can greatly affect film surface coverage. At low drop spacing values (small distance between droplets, e.g. 10 μm), the nanoparticles in each droplet exhibit large overlap, while at high drop spacing values (large distance between droplets, e.g. 100 μm), there is little to no overlap (Figure 2a). Smaller droplet spacing means more droplets are printed (higher droplets per inch, dpi) to cover the desired print area with small droplet spacing than with larger droplet spacing, which also translates to thicker films (assuming all nanoparticles immediately deposit on the surface). Pattern resolution and coverage both depend on drop spacing, so ensuring drop spacing optimization is essential. Proper drop spacing values are highly ink and substrate specific and rely on parameters such as the as surface free energy of the substrate surface, substrate surface roughness and surface tension of the ink.

Understanding the ramifications of layer number (also known as printing passes) is more straightforward. Assuming all printed nanoparticles immediately fall from suspension onto the substrate surface and are not re-dispersed upon subsequent depositions, a

homogeneous coating is achieved and thickness linearly increases with number of passes (for example: 1 pass = 40 nm, 2 passes = 80 nm, etc., Figure 2b). In the case of heterogeneous or incomplete distribution, subsequent depositions after the first might fill the space between previously printed particle aggregates, which theoretically can result in higher surface roughness (Figure 2b).

The morphological ramifications of varying both drop spacing and number of passes were investigated by mechanical profilometry when printing with an ink containing 2.1% (w/v) of TiO_2 paste. No large differences in morphology were observed between drop spacings of 20 and 35 μm. Individual printed lines were observed by the naked eye starting at a drop spacing of 50 μm, which indicated poor film homogeneity. Making one pass at a drop spacing of 25 μm resulted in an average film thickness of ~55 nm, while two passes yielded an average film thickness of ~90 nm, and three passes yielded an average film thickness of ~130 nm as measured by mechanical profilometry. Measuring a film with the same drop spacing and two passes by scanning electron microscopy indicated a film thickness of ~90-100 nm (Figure 2c).

Perovskite Solar Cell Performance

After observing how layer thickness changed with drop spacing (DS) and the number of passes, we fabricated full perovskite devices incorporating the printed TiO_2 layers with a TiO_2 paste concentration of 2.8 % (w/v). The first series of cells we fabricated focused on understanding how device performance changed with drop spacing using single pass printed films. (Table 2). PCE values for the devices ranged from 11.01% for DS = 25 to 11.84% for DS = 35. Fill Factor values ranged from 65.5 for DS = 35 to 58.2 for DS = 25. Short circuit current (J_{sc}) values ranged from 17.36 $mA \cdot cm^{-2}$ for DS 30 to 19.16 $mA \cdot cm^{-2}$ for DS = 25. Open circuit voltage (V_{oc}) values ranged from 987 mV for DS = 25 to 1018 for DS = 35. From these results, the highest V_{oc} and FF was observed for DS = 35, but the J_{sc} was not as high as for DS = 25. Because the J_{sc} and FF of these cells were low, we lowered the concentration of TiO_2

paste in the ink from 2.8 % to 2.1% to deposit a thinner TiO_2 film. Further lowering the concentration by small increments to 1.4% did not result in significant differences in device performance.

Next, we sought to better understand how device performance changed with increasing number of passes. We chose the middle drop spacing values from above (DS 25, 30) and chose to fabricate devices using between 1 and 6 passes (Table S3 and Figure S2). In general, adding layers lowered the device J_{sc} and FF values. The FF values for each of the devices was rather low, which contributed to the modest performance.

To increase inter-particle connectivity between the compact and mesoporous TiO_2 layers, we added two percent (v/v) TAA solution (75 % in isopropanol) to the ink and deposited mesoporous TiO_2 layers with and without TAA additive with varying drop spacing values and number of passes (Table S4 and Figure S3). When using a single pass, the devices without TAA additive (Drop spacing = 25, 30, and 35) all led to <13% PCE, while addition of TAA led to an increase in efficiency due to enhanced J_{sc} and FF values. The largest enhancement was observed when using a drop spacing of 25 and TAA with a single pass, with PCE values increasing from 12.56% to 16.1%. Each device with TAA exhibited increased FF and V_{oc} values over the devices without TAA. Similarly, in nearly every device (excluding Table S4 Entries 6 and 6*), the J_{sc} values also increased with TAA addition, which indicates lower recombination rates and lower series resistance across the film.

Having confirmed that TAA was beneficial for solar cell performance, we sought to better understand how substrate temperature during printing affected solar cell performance. We deposited the mesoporous TiO_2 on substrates warmed to either 45ºC or at 60ºC for facilitated ink carrier evaporation and compared them to data from Table S4, where deposition temperature was 35ºC. (Table 5). Increasing substrate temperature from 35ºC to 60ºC (Table

S5 Entry 1 vs Table S5 Entry 2 vs Table S5 Entry 3) through enhancement of J_{sc} and FF values. We reasoned that at higher substrate temperature, the evaporation rate of ink from the center of the deposited droplet forced an enhanced Marangoni ink from the droplet edges to the center. With strong Marangoni flow, the coffee ring effect is reduced and the surface coverage of nanoparticles can be thought to exhibit a convex surface morphology instead of the concave surface morphology that comes with an enhanced coffee ring effect.

To better understand the effect of TAA addition on the TiO2 film morphology, we measured the deposited films by scanning electron microscopy. We compared the top-view surface images of compact TiO_2 films deposited by spray pyrolysis, TiO_2 films deposited by inkjet printing without TAA additive, and TiO_2 films deposited by inkjet printing with TAA additive (Figure 3). The spray pyrolysis deposited compact TiO_2 layer (Figure 3a) exhibited complete and thin surface coverage, with a surface that appeared rough due to the presence of nanometer sized bumps. For the inkjet-printed mesoporous TiO_2 film (Figure 3b), the surface of the compact layer was sparsely covered by small areas of sintered nanoparticles that were sized 30 nm. Some of these nanoparticles were aggregated in such a way that the aggregates could be considered mesoscopic. Instead of a densely covered mesoporous network, as is observed with spin-coated mesoporous films,[26] the coverage was more similar to an open-pore type of network with shallow required interpenetration depths. For the inkjet-printed mesoporous TiO_2 film with TAA additive (Figure 3c), small nanoparticles (<2-10 nm), which were expected to be derived from TAA, were observed to cover the surface entirely, with sparse areas of mesoporous and free-standing TiO_2 composed of ~30 nm particles, derived from the commercial TiO_2 paste. This indicated that the addition of the TAA led to a better connected open-pore network of nanoparticles.

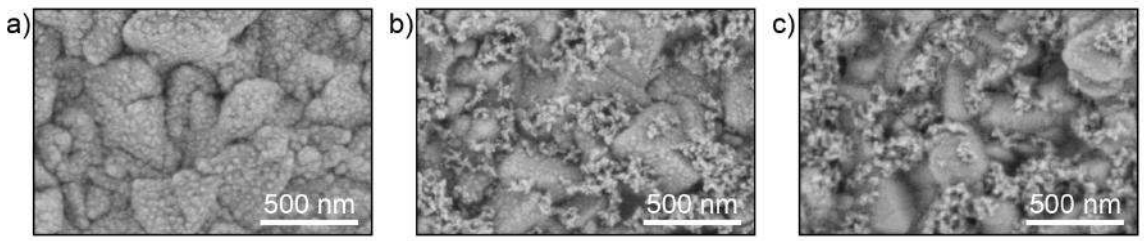

Figure 3. Scanning electron micrograph image of a) spray-pyrolysis deposited compact TiO_2 b) mesoporous TiO_2 films deposited by inkjet printing and c) mesoporous TiO_2 films deposited by inkjet printing with TAA additive.

Once the deposition conditions were optimized and the morphology of the printed film characterized, we fabricated devices utilizing either mixed $(FA_{0.15}MA_{0.85})Pb(I_{2.55}Br_{0.45})$ or pure $MAPbI_3$ and either spin-coated or inkjet-printed TiO_2 layers (Table 1). The J-V data for these comparisons are shown in Figure 4.

Table 1. Photovoltaic performance of perovskite solar cells utilizing inkjet-printed mesoporous TiO_2 layers under 100 $mW \cdot cm^{-2}$ simulated solar irradiation. Each value is an average of measurements from at least two devices. For these cells, drop spacing = 30 μm, passes = two. Asterisk denotes reference devices.

Entry	Substrate Temperature (ºC)	Perovskite	J_{sc} ($mAcm^{-2}$)	V_{oc} (mV)	FF (%)	PCE (%)
1	n/a	$MAPbI_3$	21.70*	1050*	74.0*	16.91*
2	45	$MaPbI_3$	21.75	1080	67.0	15.63
3	60	$MaPbI_3$	22.27	1050	76.0	17.78
5	45	$FA_{0.15}MA_{0.85}PbI_{2.55}Br_{0.45}$	21.09	1042	69.5	15.26

6	60	$FA_{0.15}MA_{0.85}PbI_{2.55}Br_{0.45}$	22.65	1058	76.3	18.29

This data shows that inkjet deposited mesoporous films for $MAPbI_3$ absorber layers, enhances the device performance due to enhancement of J_{sc}, and FF values when substrate temperature is 60ºC during deposition (Entry 1 vs Entry 3). When using mixed formanidinium-methylammonium iodide-bromide perovskite, the results were also improved for inkjet-printed mesoporous layer compared to the spin-coated ETL through enhancement of FF, J_{sc}, and V_{oc} values. Neither inkjet-printed nor spin-coated ETL layers were doped with Li^+ ions, which indicates that charge collection was inherently much better for the inkjet printed layer. To confirm that no adventitious Li^+ was present in the ink, we performed inductively couple plasma-optical emission spectroscopy measurements and confirmed the concentration of Li^+ present in the ink before printing was <1 ppm, while solutions typically used to dope mesoporous TiO_2 by spin-coating have >300 ppm Li^+. Obtaining high efficiency values without doping is notable, as Li^+ treatment is often reported as a necessary fabrication step for high efficiency perovskite solar cells.[27]

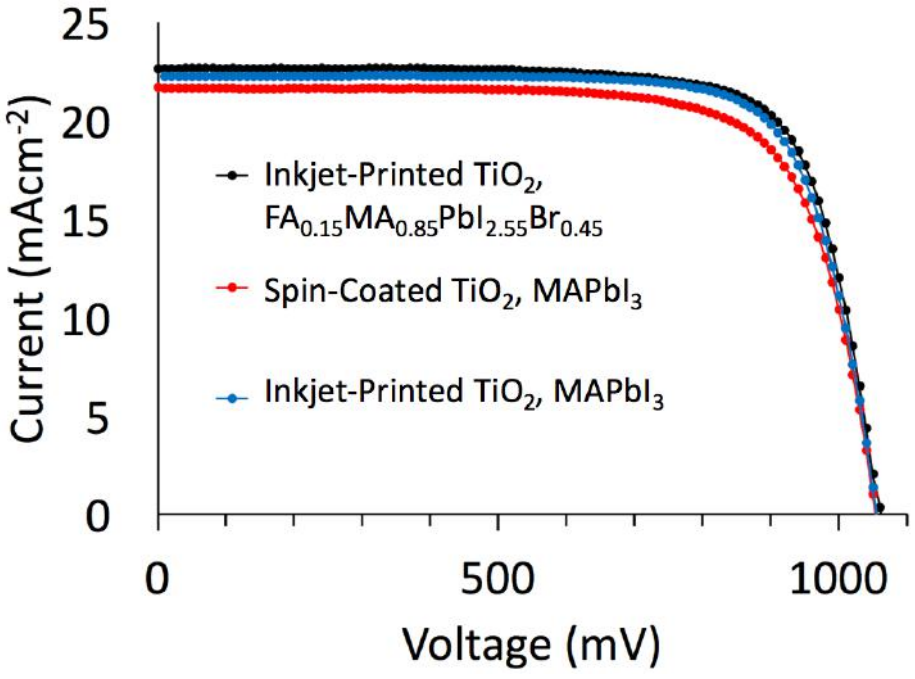

Figure 4. J-V curves of cells using spin-coated and inkjet-printed mesoporous TiO_2 cells and *Red*: Spin-coated TiO_2, *Blue*: Inkjet Printed TiO_2 and $MAPbI_3$, and *Black*: $(FA_{0.15}MA_{0.85})Pb(I_{2.55}Br_{0.45})$.

Perovskite Film Morphology

After optimization of the inkjet-printed TiO_2 film, we investigated the inkjet-printing deposition protocol for the perovskite absorber layer. Preliminary deposition trials indicated that the optimum ink formulation for perovskite printing was 33% N,N-dimethylformamide (DMF): 28% dimethylsulfoxide (DMSO): 33% γ-Butyrolactone (GBL): 5% N-methylpyrrolidone (NMP). This solvent mixture was observed to provide good wetting on the inkjet-printed TiO_2 film surface, but there was a substantial coffee ring effect[8] that resulted in inhomogeneous ink coverage and difficult-to-control film thickness. The addition of 0.1% (m/m) surfactant (phosphatidylcholine) into the ink resulted in much better film morphology control.

For the perovskite absorber composition, we chose to use a mixture of four cations: methylammonium (MA), formamidnium (FA), Cs, and guanidinium (Gu). Guanidinum has been shown to greatly enhance the stability of perovskite films when included in $MAPbI_3$ absorber layers,[28] and Cs is well known to stabilize the doubly-mixed perovskite absorber.[29] Therefore, we envisaged that the inclusion of all four cations would increase stability even further, which is important when processing films in ambient conditions. The final composition was as follows: $Cs_{0.10}Gua_{0.05}FA_{0.83}MA_{0.17}PbI_{2.63}Br_{0.37}$.

Once deposited, processing the inkjet-printed ink into a highly crystalline perovskite film is a non-trivial prospect, with many approaches in the literature reported so far, including thermal annealing,[14] photonic curing,[30] and vacuum-assisted thermal annealing.[31] During our studies, we tried several different methods of processing the films and found that anti-solvent

dipping worked the best for generating a smooth, homogenous perovskite film. We found that application of an anti-solvent, in this case dipping in diethyl ether (one of many solvents tested), for 5-10s was sufficient to generate the intermediate perovskite species and remove excess ink so that the film could then be annealed to yield a highly crystalline perovskite film.

When printing with a single pass, the thickness of the perovskite absorber layer increased with decreasing drop spacing, due to the increasing amount of ink deposited on the substrate (Figure S6). The observed films exhibited a smooth surface and were homogeneous across the printed area. The prevalence of pinholes in the film increased with increasing drop spacing, due to the decreasing amount of ink present and the distance between each printed droplet.

The optical absorption of each film was then measured by UV-Vis-NIR spectrsocopy (Figure S7, *Left*). Generally, decreasing drop spacing values (more deposited ink) resulted in an increase in film absorption. As the amount of ink increased by decreasing the drop spacing from 45 μm to 25 μm, the sharp optical transition near 800 nm increased in absorbance and indicated that the film was highly crystalline in nature. The powder X-Ray Diffraction (figure S7, *Right*) spectrum also indicated a highly crystalline perovskite film with nelgligible PbI_2 as evidenced by the minute peak near 12.9°. The diffraction spectrum very nearly matched that of previously reported Cs containing triple-cation perovskite absorber film, which indicated that the guanidinum cation did not greatly distort the lattice.[29]

We fabricated full perovskite devices incorporating the printed perovskite absorber and TiO_2 layers. First, we focused on understanding how the concentration of perovskite precursor in the ink affected device performance (Table S6, Figure S8). In general, the observed Jsc increased with increasing concentration due to increased absorber thickness (from 10.69 $mAcm^{-2}$ for 0.60 M to 18.68 $mAcm^{-2}$ for 1.2 M), while the Voc and FF was highest for 0.92 M (1007 mV and 68.2 % fill factor). Observed PCE values followed the same trend, with 4.71% PCE for 0.60 M, 12.15% PCE for 0.92 M, and 9.34% PCE for 1.2 M ink concentration.

Next, we investigated how performance changed with drop spacing using single pass printed films. (Table 2, Figure 5). PCE values for the devices ranged from 10.71% for DS = 35 to 4.64% for DS = 25. Fill Factor (FF) values ranged from 63.1 for DS = 35 to 53.3 for DS = 25. Short circuit current (J_{sc}) values ranged from 18.30 mA·cm^{-2} for DS 35 to 11.18 mA·cm^{-2} for DS = 25. Open circuit voltage (V_{oc}) values ranged from 917 mV for DS = 35 to 753 for DS = 25. From these results, the highest $V_{oc}$and FF was observed for DS = 35, the highest J_{sc} for DS = 30, and the lowest V_{oc} and Jsc observed for DS = 25, while the lowest FF observed was for DS = 30.

Table 2. Photovoltaic performance of perovskite solar cells utilizing inkjet printed mesoporous TiO_2 layers under 100 mW·cm^{-2} simulated solar irradiation. Each value is an average of measurements from at least three devices.

Drop Spacing [dpi] (μm)	J_{sc} (mA·cm^{-2})	V_{oc} (mV)	FF (%)	PCE (%)
25 [1270]	18.32	753	53.1	4.64
29 [876]	13.16	807	57.5	6.14
30 [897]	18.62	768	47.5	7.07
31 [819]	15.26	951	66.7	9.33
35 [726]	16.19	1007	68.2	12.15

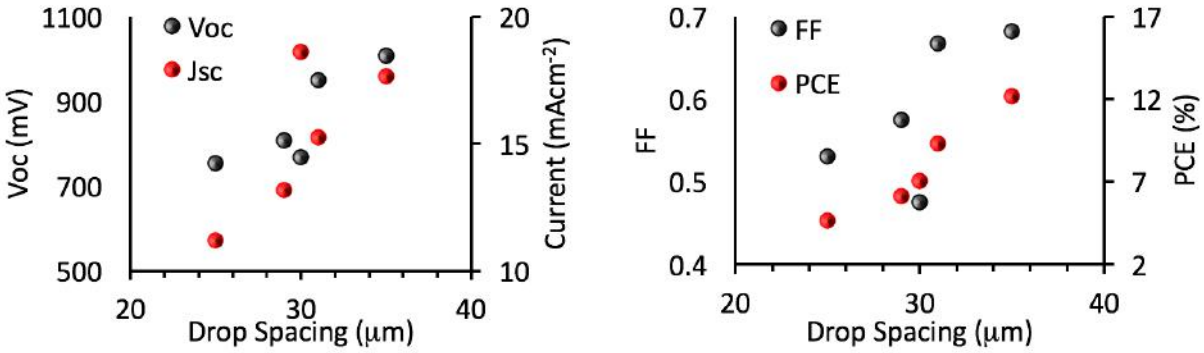

Figure 5. Performance of perovskite solar cells using inkjet-printed perovskite absorber and mesoporous TiO_2 layer at different drop spacing values. Comparison of *Left*) V_{oc} (red) and J_{sc} (black) and *Right*) comparison of FF (red) and PCE (black).

As has also been noted by others recently,[31] the observed FF values for these inkjet-printed perovskite solar cells (68.2% at DS = 35) are nearly 10% lower than was reported by Saliba et al. (77%) for films with Cs included,[29] as well as those reported by Jodlowski et al. for films with Gu included.[28] The champion cell from this study was printed with DS = 35 μm and exhibited 14.1% PCE, with Voc = 1.028 V, Jsc = 19.35 $mAcm^{-2}$, and FF = 71.0% (Figure 6), but if the FF was 77% the efficiency would have been 15.13%, which clearly shows how important reducing parasitic resistances are in these cells. With optimization of deposition and film processing, this figure should improve. The continuous power output of a typical cell was measured (Figure S9) and was found to be stable at nearly 12% PCE for 120s of maximum power point tracking, which is near the stabilized 12.9% power output reported recently for an inkjet-printed triple-cation absorber.[31] The cells tested in this study were randomly chosen from their respective batches and were not encapsulated prior to testing in ambient conditions under one sun illumination. This result indicates that the quadruple cation absorber is much more stable than the single cation $MAPbI_3$. In contrast with the quadruple cation absorber, similarly fabricated inkjet-printed $MAPbI_3$ films degraded from just over 9% PCE for a champion cell

to just over 8% PCE (Figure S9). In preliminary deposition studies of the $MAPbI_3$ films, both anti-solvent dipping and methylamine gas treatment were applied to the printed and dried films, but the highest performance and reproducibility was obtained when methylamine gas treatment was applied after thermal drying of printed ink. Concentration was important when printing these films (Figure S10). The observed Jsc, Voc, and FF all increased when the concentration of the precursor ink was increased from 0.37 M to 1.17 M, however, only the Voc increased with further concentration increase to 1.47 M. Increasing concentration led to an increase in absorber layer thickness, as more perovskite precursor was deposited, similar to the relationship in Figure S6. This thickness increase improved surface coverage, decreased apparent pinholes, and improved light absorption, however, it also decreased the observed Jsc and FF upon increasing the concentration from 1.17 M to 1.47 M.

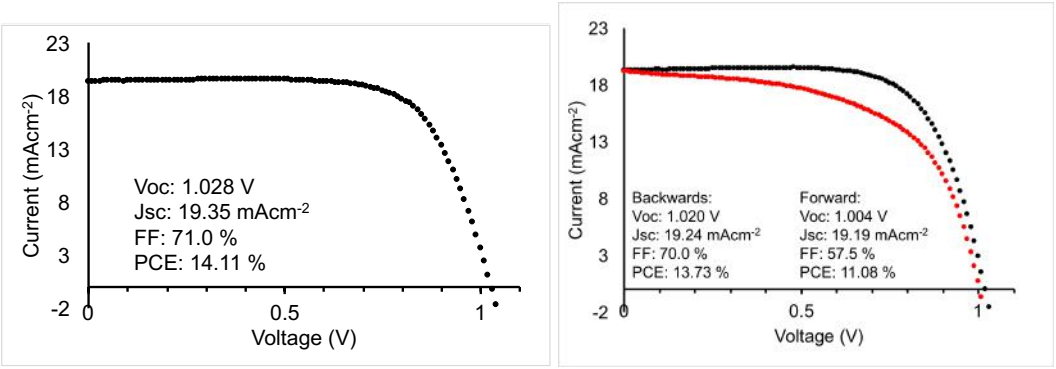

Figure 6. (*Left*): J-V curve of the champion cell resulting from the study described in Table 2. Cell illuminated with 100mWcm^{-2} of a simulated solar spectrum. (*Right*): Backwards and Forwards J-V scan illustrating the observed hysteresis present in the typical inkjet-printed perovskite solar cell in this study (DS = 35 mm, 1 pass). Cell illuminated with 100mWcm^{-2} of a simulated solar spectrum.

Typical cells from this batch exhibited hysteretic behavior, with the backward scan exhibiting 13.73% PCE and the forward scan exhibiting 11.08 % PCE. The main difference

between the two scans was due to the fill factor, which was much higher for the backwards (70.0%) than the forwards scan (57.5%, Figure 6 (*Right*)). It is expected that with further device optimization, this hysteretic behavior can be reduced. The efficiency reported here is not the highest reported for inkjet-printed perovskite solar cells, but it is the highest reported efficiency for perovskite solar cells including inkjet-printed TiO_2 and perovskite absorber layers.

Conclusions

Small scale (<1 cm^2 active area) perovskite solar cells have surpassed 22% power conversion efficiency (PCE) and reports of different techniques and architectures capable of achieving >20% PCE are increasing. To upscale perovskite solar cell fabrication, deposition steps relying on spin-coating need to be changed to scalable methods, such as printing or thermal evaporation. Inkjet printing can offer a scalable and reliable alternative to spin-coating and is already used to coat a variety of substrates on large scale. Here, we investigated the inkjet printing deposition of mesoporous TiO_2 and perovskite absorber layers. After significant device optimization studies, the performance of cells with either spin-coated or printed TiO_2 films were compared. Remarkably, devices with inkjet-printed TiO_2 (18.29 %) performed better than those with spin-coated films (16.91%), with neither film being Li^+ doped prior to perovskite deposition. Thereafter, a quadruple cation perovskite absorber was inkjet-printed onto the inkjet-printed TiO_2 film, and after some optimization trials, an average of 12.15% PCE was observed, with the champion cell yielding 14.11% PCE.

Experimental Section:

General Considerations:

All commercially available reagents were purchased and used as received. Inkjet printing and optical characterization of printed films and ejected droplets were performed using a Dimatix DMP-2850 inkjet printer equipped with disposable cartridges containing 16 nozzles. Viscosity measurements were performed using an SV-1A series viscometer (A & D). Surface Tension (pendant and sessile drop) measurements were performed using a Drop Shape Analyzer DA30S (Krüss, Germany).

Ink Synthesis: PEG-400 (0.20 mL), cyclohexanol (0.65 mL), N,N-dimethylformamide (0.15 mL) and GreatCell Solar Italia-NRT 30 TiO_2 paste (0.028 g) were combined, sonicated, and stirred at room temperature until thoroughly mixed. The suspension was then filtered through a 1.2μm filter.

Electrode preparation with compact TiO_2: Chemically etched FTO glass (Nippon Sheet Glass) was sequentially cleaned by sonication in a 2 % Helmanex solution, deionized water, acetone and isopropanol for 8 min each. To form a 30 nm thick TiO_2 blocking layer, diluted titanium di-isopropoxide bis(acetylacetonate) (TAA, 75% in isopropanol) solution (Sigma-Aldrich) was diluted in ethanol 3% (v/v) was deposited by spray pyrolysis at 450 °C.

Procedure for Spin-Coating mesoporous TiO_2: A commercially available TiO_2 paste (Dyesol 30NRT) was diluted in ethanol to 12% (w/w) and spin-coated onto the compact TiO_2 electrode. Substrates were baked at 500 ^{o}C for 30 min.

Procedure for Inkjet printing of mesoporous TiO_2: The TiO_2 ink was added to a disposable Dimatix (DMP-2800) 1.5 mL printer cartridge of nominally 10 pL jetted droplet volume and containing 16 nozzles (21 μm orifice) and nozzle spacing of 254 μm. The cartridge head was warmed to 70ºC and the substrate was warmed to 35ºC. After printing, the substrate was warmed to 100ºC for 10 min and then baked at 500ºC for 30 min. The annealed substrates were then scored to yield 1.35 x 2.35 cm^2 areas. When fabricating spin-coated perovskite layers on these electrodes, the substrate was broken along the scored lines. When inkjet-printing the

perovskite layer on these electrodes, the substrate was not broken along the scored lines until the perovskite was deposited.

Perovskite Deposition:

Mixed-perovskite precursor was prepared by mixing 1.15 M PbI_2, 1.10 M FAI, 0.2 M $PbBr_2$, 0.2 M MABr in a mixed solvent of DMF:DMSO = 4:1 (volume ratio). Mixed perovskite solutions were successively spin-coated in the glovebox as follows: first, 2000 rpm for 10 s with a ramp-up of 200 rpm·s^{-1}; second, 6000 rpm for 30 s with a ramp-up of 2000 rpm· s^{-1}. Toluene (110 μl) was dropped on the spinning substrate during the second spin-coating step 20 s before the end of the procedure. Then films were annealed at 100 ^{o}C for 90 min.

The pure $MaPbI_3$ precursor solution contained 1.3 M PbI2 and 1.3 M MAI in anhydrous DMSO. The perovskite films were prepared by spin-coating on the substrates at 1000 rpm for the first 10 s and 4000 rpm for the following 30 s. Chlorobenzene (0.1 mL, CB) was slowly dropped on the film 10 s before the spin-coating program finished, then the samples were heated at 100°C for 1 h.

Perovskite Ink Synthesis:

Quadruple Cation Absorber: The perovskite precursor ink was prepared by first mixing PbI_2 (1.15 mmol, 0.53 g), FAI (1.033 mmol, 0.177 g), $PbBr_2$ (0.19 mmol, 0.071 g), MABr (0.18 mmol, 0.020 g), GuI (0.063 mmol, 0.012 g), and phosphatidylcholine (0.001 g) in a mixed solvent of DMF:DMSO:GBL:NMP = 33:28:33:5 (volume ratio). Separately, CsI (1.15 mmol, 0.299 g) and PbI_2 (1.15 mmol, 0.53 g) were mixed together and dissolved in a mixed solvent of DMF:DMSO:GBL:NMP = 33:28:33:5 (volume ratio). The two solutions were then mixed to give a 10:1 ratio. Best results were obtained with fresh solutions.

$MAPbI_3$ Absorber: The perovskite precursor ink was prepared by first mixing PbI_2 (1.15 mmol, 0.53 g), MAI (1.15 mmol, 0.181 g), and phosphatidylcholine (0.001 g) in a mixed solvent of

DMF:DMSO:GBL:NMP = 33:28:33:5 (volume ratio). Best results were obtained with fresh solutions.

Procedure for Inkjet Printing of the Perovskite Absorber: The perovskite ink was loaded into a disposable Dimatix (DMP-2800) 1.5 mL printer cartridge of nominally 10 pL jetted droplet volume and containing 16 nozzles (21 μm orifice) and nozzle spacing of 254 μm. The cartridge head and substrate were not warmed prior to printing. Once printed, the wet film was immersed in diethyl ether for 5-10 s, removed, and annealed at 120ºC in ambient conditions.

Hole Transport Material (HTM) Deposition and gold evaporation: HTM solution (40 μL) containing 91 mg Spiro-OMeTAD and additives (21 μL of Li-bis(trifluoromethanesulfonyl)imide from a stock solution of 520 mg in 1 mL of acetonitrile, 16 μL of FK209, tris(2-(1H-pyrazol-1-yl)-4-tert-3 butylpyridine)-cobalt(III) tris(bis(trifluoromethylsulfonyl)imide from a stock solution of 375 mg in 1 mL of acetonitrile, and 36 μL of 4-tertbutylpyridine) in 1 mL of CB was spin-coated on the samples at 4000 rpm for 20 s, and followed by the evaporating Au electrode with thickness of 70 nm.

Photovoltaic Characterization: The photovoltaic performance was analyzed using a VeraSol LED solar simulator (Newport) coupled with a Keithley 2400 source/meter giving light with AM 1.5G (100 W/cm^2) spectral distribution. A black mask with an aperture 0.16 cm^2 was applied on top of the cell. The light intensity was calibrated with an NREL certified KG5 filtered Si reference diode.

Acknowledgements

A.H would like to thank the Toyota Motor Company and the US Army (grant agreement No. W911NF-17-2-0122). A.H. would also like to thank Daniel T. Sun for help with ICP-OES measurements. We thank Borun New Material Technology for providing high quality spiro-OmeTAD.

References

(1) Kojima, A.; Teshima, K.; Shirai, Y.; Miyasaka, T. Organometal Halide Perovskites as Visible-Light Sensitizers for Photovoltaic Cells. *J. Am. Chem. Soc.* **2009**, *131* , 17, 6050–6051.

(2) Zhang, W.; Eperon, G. E.; Snaith, H. J. Metal Halide Perovskites for Energy Applications. *Nat. Energy* **2016**, *1* , 6, 16048.

(3) Williams, S. T.; Rajagopal, A.; Chueh, C. C.; Jen, A. K. Y. Current Challenges and Prospective Research for Upscaling Hybrid Perovskite Photovoltaics. *J. Phys. Chem. Lett.* **2016**, *7* , 5, 811–819.

(4) Wang, J.; Giacomo, F. Di; Brüls, J.; Gorter, H.; Katsouras, I.; Groen, P.; Janssen, A. J.; Andriessen, R.; Galagan, Y. Highly Efficient Perovskite Solar Cells Using Non-Toxic Industry Compatible Solvent System. **2017**, *1700091*, 1–9.

(5) Ávila, J.; Momblona, C.; Boix, P. P.; Sessolo, M.; Bolink, H. J. Vapor-Deposited Perovskites: The Route to High-Performance Solar Cell Production? *Joule* **2018**, *1* , 3, 431–442.

(6) Mathies, F.; Abzieher, T.; Hochstuhl, A.; Glaser, K.; Colsmann, A.; Paetzold, U. W.; Hernandez-Sosa, G.; Lemmer, U.; Quintilla, A. Multipass Inkjet Printed Planar Methylammonium Lead Iodide Perovskite Solar Cells. *J. Mater. Chem. A* **2016**, *4* , 48, 19207–19213.

(7) Grancini, G.; Roldán-Carmona, C.; Zimmermann, I.; Mosconi, E.; Lee, X.; Martineau, D.; Narbey, S.; Oswald, F.; De Angelis, F.; Graetzel, M.; et al. One-Year Stable Perovskite Solar Cells by 2D/3D Interface Engineering. *Nat. Commun.* **2017**, *8*, 15684.

(8) Derby, B. Inkjet Printing of Functional and Structural Materials : Fluid Property Requirements , Feature Stability , and Resolution. *Annu. Rev. Mater. Res.* **2010**, *40* , 395–414.

(9) Shu, Z.; Beckert, E.; Eberhardt, R.; Tunnermann, A. ITO-Free{,} Inkjet-Printed Transparent Organic Light-Emitting Diodes with a Single Inkjet-Printed Al:ZnO:PEI Interlayer for Sensing Applications. *J. Mater. Chem. C* **2017**, *5* , 44, 11590–11597.

(10) Carey, T.; Cacovich, S.; Divitini, G.; Ren, J.; Mansouri, A.; Kim, J. M.; Wang, C.; Ducati, C.; Sordan, R.; Torrisi, F. Fully Inkjet-Printed Two-Dimensional Material Field-Effect Heterojunctions for Wearable and Textile Electronics. *Nat. Commun.* **2017**, *8* , 1, 1202.

(11) Eggenhuisen, T. M.; Galagan, Y.; Biezemans, A. F. K. V; Slaats, T. M. W. L.; Voorthuijzen, W. P.; Kommeren, S.; Shanmugam, S.; Teunissen, J. P.; Hadipour, A.; Verhees, W. J. H.; et al. High Efficiency{,} Fully Inkjet Printed Organic Solar Cells with Freedom of Design. *J. Mater. Chem. A* **2015**, *3* , 14, 7255–7262.

(12) Peng, X.; Yuan, J.; Shen, S.; Gao, M.; Chesman, A. S. R.; Yin, H.; Cheng, J.; Zhang, Q.; Angmo, D. Perovskite and Organic Solar Cells Fabricated by Inkjet Printing: Progress and Prospects. *Adv. Funct. Mater. 27* , 41, 1703704.

(13) Bag, M.; Jiang, Z.; Renna, L. A.; Jeong, S. P.; Rotello, V. M. Rapid Combinatorial Screening of Inkjet-Printed Alkyl-Ammonium Cations in Perovskite Solar Cells. *Mater. Lett.* **2016**, *164*, 472–475.

(14) Li, S.-G.; Jiang, K.-J.; Su, M.-J.; Cui, X.-P.; Huang, J.-H.; Zhang, Q.-Q.; Zhou, X.-Q.; Yang, L.-M.; Song, Y.-L. Inkjet Printing of CH3NH3PbI3 on a Mesoscopic TiO2 Film for Highly Efficient Perovskite Solar Cells. *J. Mater. Chem. A* **2015**, *3* , 17, 9092–9097.

(15) Hashmi, S. G.; Martineau, D.; Li, X.; Ozkan, M.; Tiihonen, A.; Dar, M. I.; Sarikka, T.; Zakeeruddin, S. M.; Paltakari, J.; Lund, P. D.; et al. Air Processed Inkjet Infiltrated Carbon Based Printed Perovskite Solar Cells with High Stability and Reproducibility. *Adv. Mater. Technol.* **2017**, *2* , 1, 1600183.

(16) Jung, S.; Sou, A.; Banger, K.; Ko, D.; Chow, P. C. Y.; Mcneill, C. R.; Sirringhaus, H. All-Inkjet-Printed , All-Air-Processed Solar Cells. **2014**, 1–9.
(17) Li, Y.; Lan, L.; Sun, S.; Lin, Z.; Gao, P.; Song, W.; Song, E.; Zhang, P.; Peng, J. All Inkjet-Printed Metal-Oxide Thin-Film Transistor Array with Good Stability and Uniformity Using Surface-Energy Patterns. **2017**.
(18) Cherrington, R.; Hughes, D. J.; Senthilarasu, S.; Goodship, V. Inkjet-Printed TiO 2 Nanoparticles from Aqueous Solutions for Dye-Sensitized Solar Cells (DSSCs). **2015**, 866–870.
(19) Wojcik, P. J.; Aguas, H.; Fortunato, E.; Martins, R. Journal of Colloid and Interface Science Inkjet Printed Highly Porous TiO 2 Films for Improved Electrical Properties of Photoanode. *J. Colloid Interface Sci.* **2016**, *465*, 208–214.
(20) Ren, Y.; Li, Y.; Chen, S.; Liu, J.; Zhang, J.; Wang, P. Improving the Performance of Dye-Sensitized Solar Cells with Electron-Donor and Electron-Acceptor Characteristic of Planar Electronic Skeletons. *Energ Environ. Sci.* **2016**.
(21) Sanghyun, P.; Peng, Q.; Yonghui, L.; Taek, C. K.; Peng, G.; Giulia, G.; Emad, O.; Paul, G.; Kasparas, R.; A., A. S.; et al. Dopant-Free Hole-Transporting Materials for Stable and Efficient Perovskite Solar Cells. *Adv. Mater.* **2017**, *29* , 35, 1606555.
(22) Bernacka-wojcik, I.; Senadeera, R.; Jerzy, P.; Bione, L.; Baptista, P.; Aguas, H.; Fortunato, E.; Martins, R. Biosensors and Bioelectronics Inkjet Printed and " Doctor Blade " TiO 2 Photodetectors for DNA Biosensors. **2010**, *25*, 1229–1234.
(23) Oh, Y.; Yoon, H. G.; Lee, S.-N.; Kim, H.-K.; Kim, J. Inkjet-Printing of TiO2 Co-Solvent Ink: From Uniform Ink-Droplet to TiO2 Photoelectrode for Dye-Sensitized Solar Cells. *J. Electrochem. Soc.* **2011**, *159* , 1, B34–B38.
(24) Pourjafari, D.; Oskam, G.; Tinoco, J. C.; Martínez-lópez, A. G.; Rodríguez-gattorno, G. Materials Science in Semiconductor Processing Stable Inks for Inkjet Printing of TiO 2 Thin Fi Lms. **2018**, *81* , January, 75–81.
(25) Gans, B. B. De; Duineveld, P. C.; Schubert, U. S. Inkjet Printing of Polymers : State of the Art and Future Developments **. *Adv. Mater.* **2004**, No. 3, 203–213.
(26) O'Regan, B.; Grätzel, M. A Low-Cost, High-Efficiency Solar Cell Based on Dye-Sensitized Colloidal TiO2 Films. *Nature* **1991**, *353*, 737–740.
(27) Giordano, F.; Abate, A.; Pablo, J.; Baena, C.; Saliba, M.; Matsui, T.; Im, S. H.; Zakeeruddin, S. M.; Nazeeruddin, M. K.; Hagfeldt, A.; et al. Enhanced Electronic Properties in Mesoporous TiO2 via Lithium Doping for High-Efficiency Perovskite Solar Cells. *Nat. Commun.* **2016**, *7*, 1–6.
(28) Jodlowski, A. D.; Roldán-Carmona, C.; Grancini, G.; Salado, M.; Ralaiarisoa, M.; Ahmad, S.; Koch, N.; Camacho, L.; de Miguel, G.; Nazeeruddin, M. K. Large Guanidinium Cation Mixed with Methylammonium in Lead Iodide Perovskites for 19% Efficient Solar Cells. *Nat. Energy* **2017**, *2* , 12, 972–979.
(29) Saliba, M.; Matsui, T.; Seo, J.-Y.; Domanski, K.; Correa-Baena, J.-P.; Nazeeruddin, M. K.; Zakeeruddin, S. M.; Tress, W.; Abate, A.; Hagfeldt, A.; et al. Cesium-Containing Triple Cation Perovskite Solar Cells: Improved Stability, Reproducibility and High Efficiency. *Energ Environ. Sci.* **2016**, *9* , 6, 1989–1997.
(30) Troughton, J.; Carnie, M. J.; Davies, M. L.; Charbonneau, C.; Jewell, E. H.; Worsley, D. A.; Watson, T. M. Photonic Flash-Annealing of Lead Halide Perovskite Solar Cells in 1 Ms. *J. Mater. Chem. A* **2016**, *4* , 9, 3471–3476.
(31) Mathies, F.; Eggers, H.; Richards, B. S.; Hernandez-sosa, G.; Lemmer, U.; Paetzold, U. W. Inkjet-Printed Triple Cation Perovskite Solar Cells. *ACS Appl. Energy Mater.* **2018**, *1* , 5, 1834–1839.

TOC: Inkjet-printing of TiO_2 and perovskite absorber layers has led to high efficiency solar cells printed over >10 cm^2.

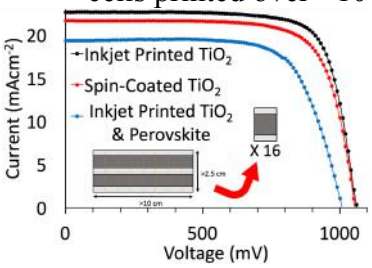

Supporting Information

Inkjet-Printed Mesoporous TiO_2 and Perovskite Layers for High Efficiency Perovskite Solar Cells

Aron J. Huckaba,[a,*] Yonghui Lee,[a] Rui Xia,[a,b] Sanghyun Paek,[a] Victor Costa Bassetto,[c] Emad Oveisi,[d] Andreas Lesch,[c] Sachin Kinge,[e] Paul J. Dyson,[b] Hubert Girault,[c] Mohammad Khaja Nazeeruddin[a],*

a: GMF, Institute of Chemical Sciences and Engineering, EPFL Valais-Wallis, Rue de l'industrie 17, 1951 Sion, Switzerland.

b: Institute of Chemical Sciences and Engineering, Ecole Polytechnique Fédérale de Lausanne (EPFL), CH-1015 Lausanne, Switzerland.

c: LEPA, Institute of Chemical Sciences and Engineering, EPFL Valais-Wallis, Rue de l'industrie 17, 1951 Sion, Switzerland.

d: Interdisciplinary Centre for Electron Microscopy, EPFL, 1015 Lausanne, Switzerland

e: Toyota Motor Corporation, Toyota Motor Technical Centre, Advanced Technology Div., Hoge Wei 33, B-1930 Zaventum, Belgium.

Table S1. Physical properties of solvents and ternary ink used in this work.

Solvent	Dynamic Viscosity (mPa·s) [T, ºC][a]	Surface Tension (dynes·cm^{-1}), [T, ºC]	Vapour Pressure (kPa) [T, ºC]	Density (g·mL^{-1}, 25ºC)[a]
Cyclohexanol	57.5 [25]	32.35 [30][26]	1.99 [70][27]	0.962
N,N-dimethylformamide	0.92 [20]	35.87 [30][28]	6.43 [70][29]	0.944

Poly(ethyleneglycol) 400	120 [20]	60 [30][30]	$1x10^{-3}$ [20]	1.128
Ternary ink blend (this work)	14.1 [25]	32.7 [25]	---	1.07

a: values taken from ref 31.

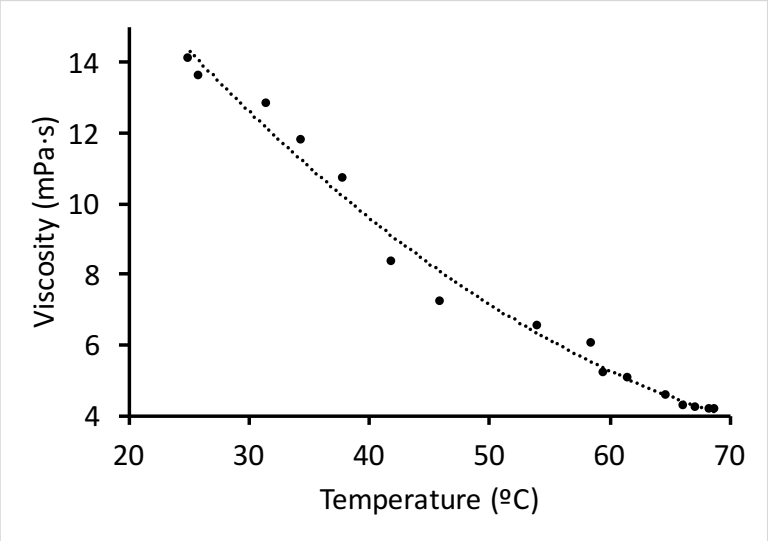

Figure S1. Measured dynamic viscosity for TiO_2 ink at a variety of temperatures. Dashed line is included to guide the eye only.

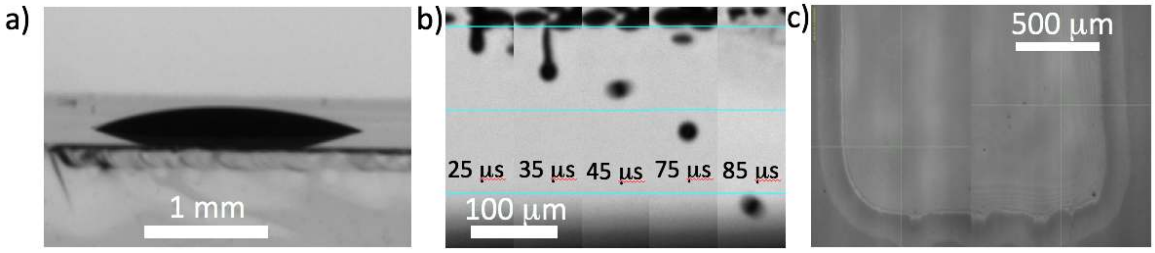

Figure S2. *a)* Sessile droplet on a cleaned compact TiO_2 surface. *b)* Droplet ejection at low driving voltages at selected time intervals. *c)* Light microscope image of printed ink on a compact TiO_2 surface using a drop spacing of 30 µm (897 dpi) and substrate temperature of 35ºC.

Table S2. Photovoltaic performance of perovskite solar cells utilizing inkjet printed mesoporous TiO_2 layers under 100 $mW \cdot cm^{-2}$ simulated solar irradiation. Each value is an average of measurements from at least two devices.

Drop Spacing [dpi] (μm)	J_{sc} ($mA \cdot cm^{-2}$)	V_{oc} (mV)	FF (%)	PCE (%)
20 [1270]	18.32	999	61.4	11.24
25 [1016]	19.16	987	58.2	11.01
30 [897]	17.36	1002	64.0	11.13
35 [726]	17.76	1018	65.5	11.84

Table S3. Photovoltaic performance of perovskite solar cells utilizing inkjet-printed mesoporous TiO_2 layers under 100 $mW \cdot cm^{-2}$ simulated solar irradiation. Each value is an average of measurements from at least two devices.

Entry	DS (μm)	Passes	J_{sc} ($mA \cdot cm^{-2}$)	V_{oc} (mV)	FF (%)	PCE (%)
1	25	1	21.81	1056	60.4	13.91
2	25	2	21.37	1048	59.5	13.32
3	25	3	21.34	1048	61.9	13.84
4	25	4	21.01	1012	59.2	12.58
5	25	5	20.05	1035	60.0	12.44
6	25	6	19.82	1014	55.1	11.07
7	30	1	21.18	1026	58.1	12.62
8	30	2	20.91	1049	61.6	13.50

9	30	3	16.30	1015	67.5	11.16
10	30	4	17.84	1008	57.8	10.40
11	30	5	17.63	1017	60.6	10.86
12	30	6	12.5	963	55.1	6.63

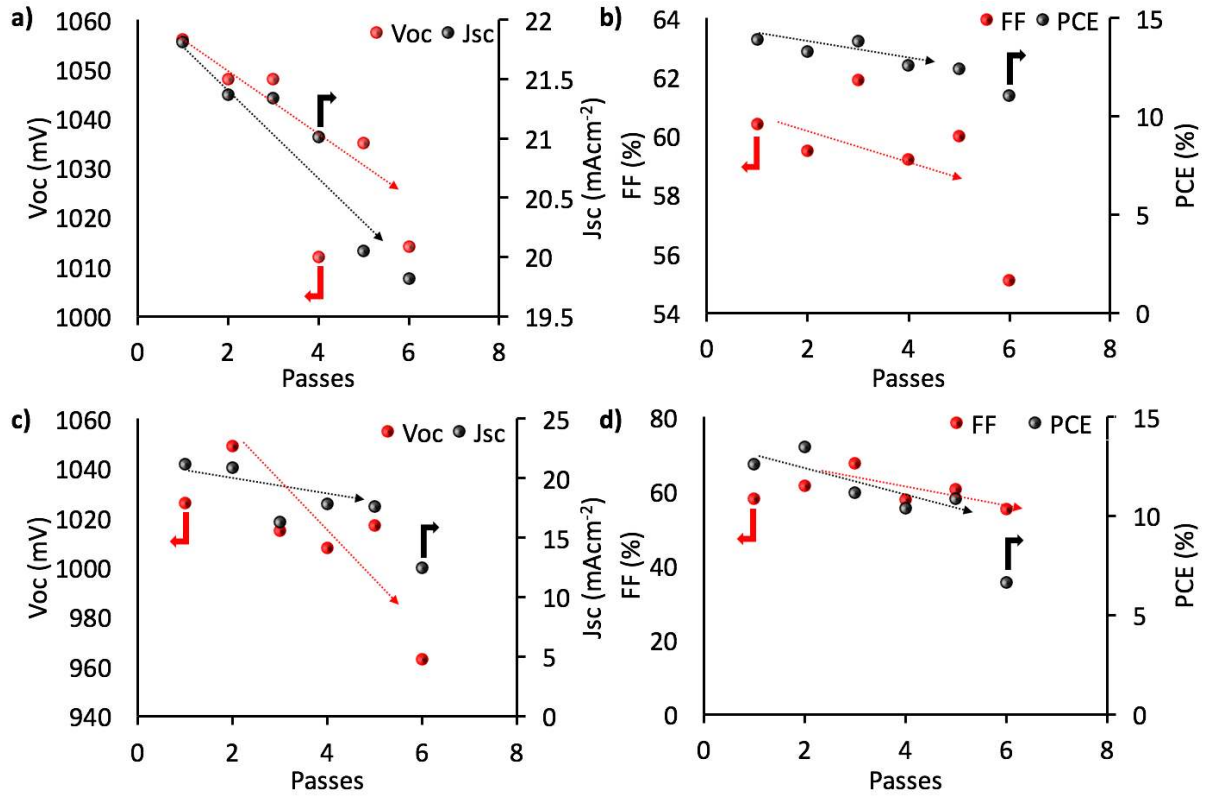

Figure S2. Performance of perovskite solar cells fabricated with inkjet-printed mesoporous TiO_2 layers using either a) and b) drop spacing of 25 μm or c) and d) drop spacing of 30 μm. Comparison of a) and c) V_{oc} (red) and J_{sc} (black) and b) and d) FF (red) and PCE (black). Dashed arrows are intended to guide the eye only.

Table S4. Photovoltaic performance of perovskite solar cells utilizing inkjet-printed mesoporous TiO_2 layers under 100 $mW \cdot cm^{-2}$ simulated solar irradiation. Each value is an average of measurements from at least two devices. Entries marked with an asterisk (*) denotes entries with added TAA.

Entry	DS (μm)	Passes	J_{sc} (mA·cm^{-2})	V_{oc} (mV)	FF (%)	PCE (%)
1	25	1	18.42	1010	62.5	12.56
1*	25	1	20.46	1110	70.8	16.1
2	30	1	19.63	1087	60.7	12.93
2*	30	1	20.77	1099	59.5	13.57
3	30	2	21.13	1101	59.7	13.89
3*	30	2	20.19	1113	63.1	14.18
4	30	3	17.68	1090	56.5	10.89
4*	30	3	21.52	1092	65.0	15.27
5	35	1	20.05	1035	60.0	12.44
5*	35	1	21.19	1098	60.1	14.1
6	35	2	22.39	1100	64.0	15.77
6*	35	2	15.83	1131	67.2	12.0
7	35	3	18.56	1079	61.6	12.30
7*	35	3	19.0	1121	62.3	13.3

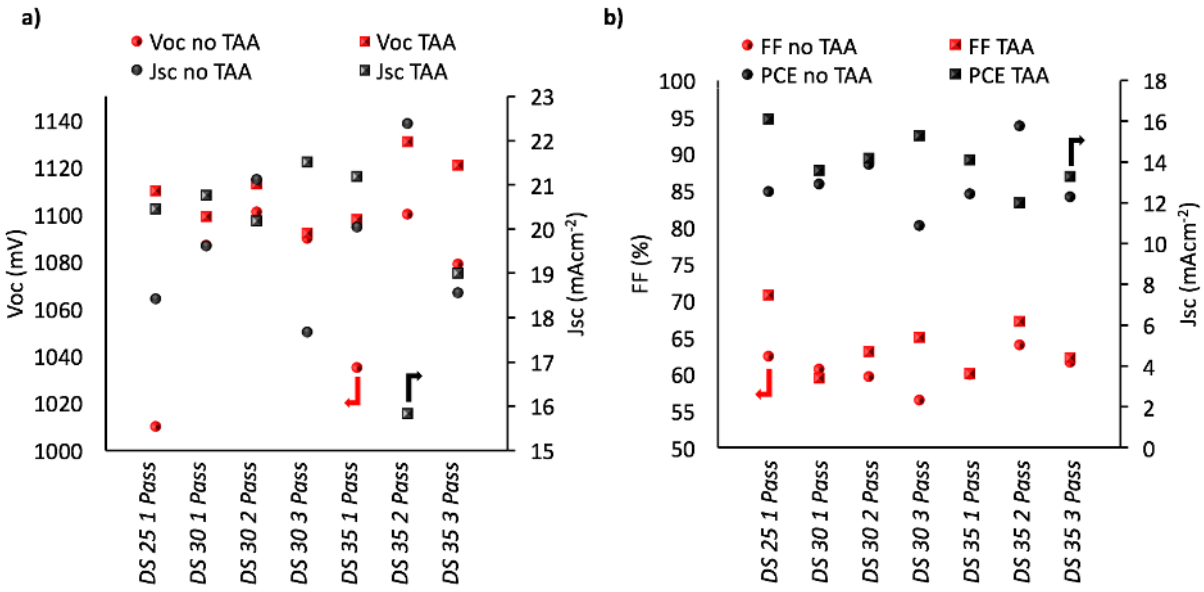

Figure S3. Performance of perovskite solar cells using inkjet-printed mesoporous TiO_2 layer without (circles) and with (squares) TAA additive. Comparison of a) V_{oc} (red) and J_{sc} (black) and b) comparison of FF (red) and PCE (black). Each data point is an average of measurements from at least two devices.

Table S5. Photovoltaic performance of perovskite solar cells utilizing inkjet-printed mesoporous TiO_2 layers under 100 $mW \cdot cm^{-2}$ simulated solar irradiation. Each value is an average of measurements from at least two devices. For these cells, drop spacing = 30 μm, passes = two. Asterisk denotes champion cell.

Entry	Substrate Temperature (ºC)	J_{sc} ($mA \cdot cm^{-2}$)	V_{oc} (mV)	FF (%)	PCE (%)
1	35	21.13	1101	59.7	13.89
2	45	21.09	1042	69.5	15.26
3	60	22.39 (± 0.30) 22.65*	1043 (± 0.025) 1058*	73.7 (± 0.021) 76.3*	17.19 (± 0.79) 18.29*

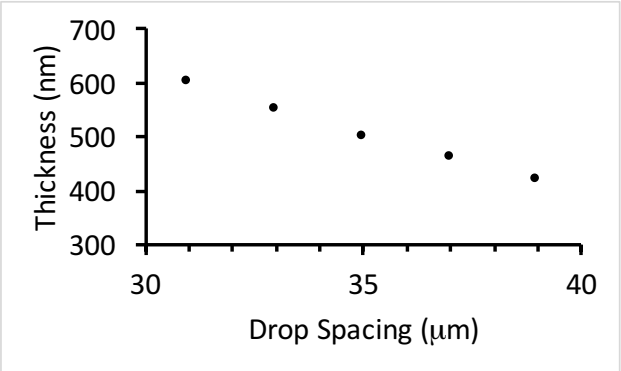

Figure S6. Change in perovskite absorber layer thickness as measured by mechanical profilometry resulting from varying the drop spacing (printing passes = 1).

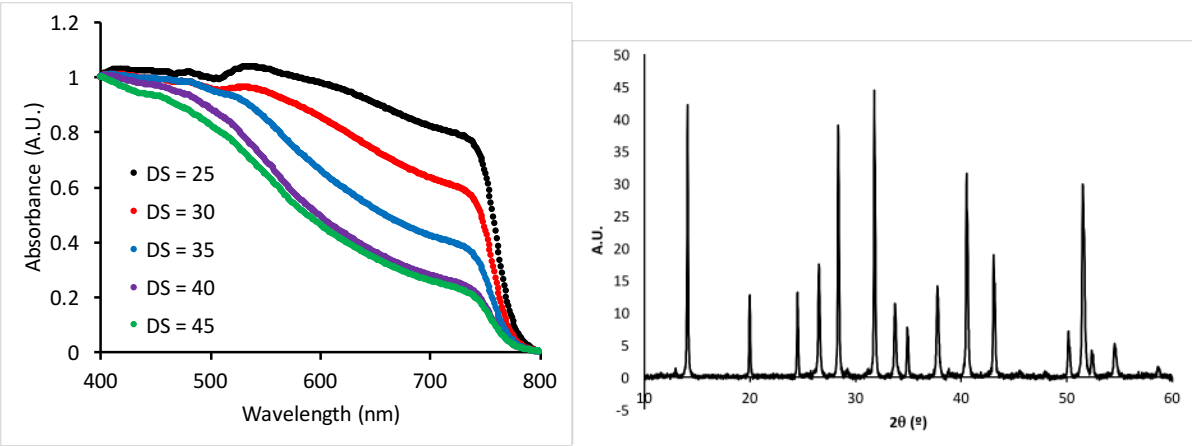

Figure S7. (*Left*): UV-Vis-NIR absorption spectrum of inkjet-printed perovskite films on inkjet-printed TiO_2 film with varying drop spacing values. (*Right*): Powder X-Ray Diffraction pattern of the inkjet-printed perovskite film on inkjet-printed TiO_2.

Table S6. Photovoltaic performance of perovskite solar cells utilizing inkjet printed mesoporous TiO_2 layers under 100 $mW \cdot cm^{-2}$ simulated solar irradiation (DS = 35 μm). Each value is an average of measurements from at least three devices.

Precursor Ink Concentration	J_{sc} ($mA \cdot cm^{-2}$)	V_{oc} (mV)	FF (%)	PCE (%)
0.60	10.69	782	54.3	4.71
0.92	16.19	1007	68.2	12.15
1.2	18.68	862	47.5	9.34

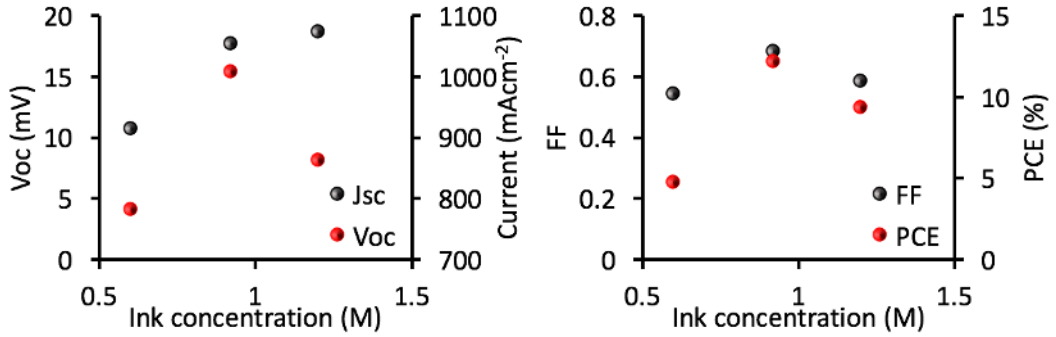

Figure S8. Performance of perovskite solar cells using inkjet-printed perovskite absorber and mesoporous TiO_2 layer at different ink precursor concentrations. Comparison of *Left*) V_{oc} (red) and J_{sc} (black) and *Right*) comparison of FF (red) and PCE (black). Each data point is an average of measurements from at least three devices.

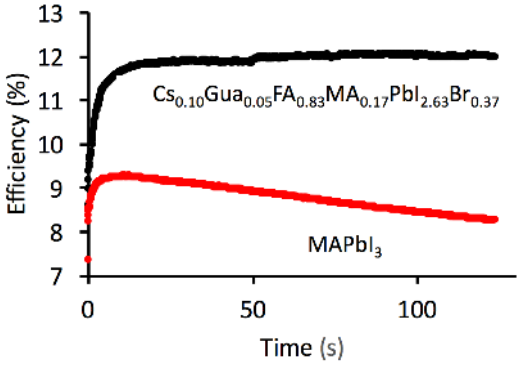

Figure S9. Continuous power output measurement of a typical quadruple cation perovskite solar cell fabricated in this study (black) compared to a similarly prepared device with $MAPbI_3$. Devices were not encapsulated and were measured in ambient conditions.

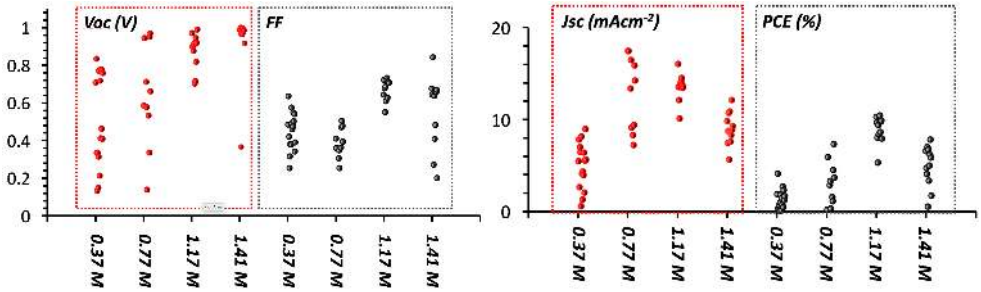

Figure S10. Performance of perovskite solar cells using inkjet-printed $MAPbI_3$ perovskite absorber with methylamine vapor treatment and mesoporous TiO_2 layer at different ink precursor concentrations. Comparison of *Left*) V_{oc} (red) and J_{sc} (black) and *Right*) comparison of FF (red) and PCE (black).